Atmospheric Environment 42 (2008) 5569–5578

Contents lists available at ScienceDirect

Atmospheric Environment

journal homepage: www.elsevier.com/locate/atmosenv

Evidence for large-scale transport of biomass burning aerosols from sunphotometry at a remote South African site

H. Winkler [a,*], P. Formenti [b,1], D.J. Esterhuyse [c], R.J. Swap [d], G. Helas [b], H.J. Annegarn [e], M.O. Andreae [b]

[a] Department of Physics, University of Johannesburg, South Africa
[b] Biogeochemistry Department, Max Planck Institute for Chemistry, Mainz, Germany
[c] South African Weather Services, Pretoria, South Africa
[d] Department of Environmental Sciences, University of Virginia, Charlottesville, VA, USA
[e] Department of Environmental Sciences, University of Johannesburg, South Africa

ARTICLE INFO

Article history:
Received 9 April 2007
Received in revised form
13 December 2007
Accepted 14 March 2008

Keywords:
Aerosol properties
Sun photometry
Angström parameter
Africa

ABSTRACT

We present the results of sunphotometry measurements at De Aar, a remote site on the central South African plateau, during and after the intensive dry season field campaign of SAFARI 2000. We determine a 6-month-long time series of aerosol optical depths over the site. Twelve haze events are identified, for which we derive Angström exponents and their derivatives, and, through cross-plots of these parameters, typical aerosol sizes and levels of hydration. These results, in conjunction with meteorological data and air trajectory calculations, show biomass burning to be the main aerosol generating source for 8 of the 12 events, and responsible for the 5 cases with the highest turbidity. While the bulk of the biomass emission is clearly of African origin, we identify several possible South Atlantic crossings of aged smoke from fires in the Amazon basin. We define the southern edge of the main aerosol transport route over southern Africa during the austral winter. We estimate that, for the half-year investigated, 84% of the losses of visible solar irradiation over our experimental location are caused by biomass burning haze, and conclude that these types of aerosols have the most critical impact on solar irradiation and atmospheric albedo over the entire southern Africa.

© 2008 Elsevier Ltd. All rights reserved.

1. Introduction

The Southern African Regional Science Initiative (SAFARI 2000) sought to determine the generation, transport and deposition of aerosols and trace gases over the southern African sub-continent, and to develop our understanding of related environmental processes, such as the effect of aerosols on the global radiation balance (Swap et al., 2002; Otter et al., 2002). Individual SAFARI 2000 projects studied and reported on biomass characteristics and emissions, aerosol inventories under a variety of conditions, a satellite validation programme, and air circulation patterns. Findings have been reviewed by Swap et al. (2003) and Shugart et al. (2004).

During the austral spring, biomass burning occurs in Africa at latitudes between the Kalahari desert and the Congo basin. Emissions from these fires are expected to occasionally reach the central South African plateau, via the Angolan and Namibian coastal regions, whenever a sub-continental anticyclone is well developed.

A recirculation of airmasses, and aerosols and trace gases therein, over southern Africa has been proposed in several studies (Garstang et al., 1996; Tyson, 1997) and tested in a number of field campaigns: SAFARI 1992

* Corresponding author. Tel.: +27 11 4892327; fax: +27 11 4892339.
E-mail address: hwinkler@uj.ac.za (H. Winkler).
[1] Now at: Laboratoire Interuniversitaire des Systèmes Atmosphériques, UMR CNRS Univ. Paris 7&12, Créteil, France.

1352-2310/$ - see front matter © 2008 Elsevier Ltd. All rights reserved.
doi:10.1016/j.atmosenv.2008.03.031

(Lindesay et al., 1996), SA'ARI 94 (Helas et al., 1995), and BHATTEX (Piketh et al., 1999). Accordingly, a goal of SAFARI 2000 was to further explore the nature and extent of the recirculative southern African atmospheric gyre. With this in mind, project leadership supported the idea of measurements at a remote South African site to determine the poleward extent of such a system.

Aerosol concentrations and size distributions can be derived remotely through solar direct beam measurements at a range of wavelengths and zenith angles. The AERONET programme (Holben et al., 1998, 2001) maintains a global network of sunphotometers for this purpose. Data from several of their Zambian stations were used to characterise the photometric properties of southern African biomass smoke in 1997 (Eck et al., 2001a).

During the SAFARI 2000 project, AERONET sunphotometers again monitored aerosols over several southern African locations (Eck et al., 2003; Elias et al., 2003; Queface et al., 2003). However, these studies restrict themselves to areas north of the Walvis Bay–Durban line, the approximate south-eastern limit of a spectacular event of aerosol flow from southern Africa out to the Indian Ocean at the beginning of September 2000, dubbed the 'River of Smoke' (see Swap et al., 2003).

One region not covered by the AERONET studies, and which furthermore coincided with the expected southern edge of the regional gyre, is the Karoo semi-desert. This paper describes sunphotometer data obtained in this area during SAFARI 2000, and examines its significance.

2. Experimental and data reduction

The Karoo region can be considered ideal for the study of long-range aerosol transport. It is sparsely populated and has no major industries or mining activities, greatly limiting local production of anthropogenic aerosols. Dust generation is reduced because of generally stony ground. Finally, it enjoys above-average sunshine hours, making it a prime site for ground-based aerosol characterisation through sunphotometry.

The town of De Aar lies in the eastern part of the Karoo. The widespread municipality of Emthanjeni recorded a population of 35,539 in the 2001 national census (about half of which live in De Aar). The town largely developed due to a major railway junction. Anthropogenic emissions in the area are however minimal, and limited to light industry and a few domestic fires. There is almost no crop farming within a 100 km radius of the town (Fig. 1).

The De Aar meteorological station (30°40′S, 24°00′E; 1287 m a.s.l.) is highly developed and well staffed. It is the South African site in the Baseline Surface Radiation Network (BSRN) (Ohmura et al., 1998), and broad-band solar irradiation measurements have been made here since July 1999 (Esterhuyse, 2004). The station is on a small hill on the south-west edge of the town. Local emissions would only affect the site in the event of wind from the east or north-east.

De Aar was hence chosen as a sunphotometer site for the duration of SAFARI 2000. These measurements continued and complemented those performed during 1998 and 1999 in Sutherland (32°22′S, 20°48′E), also in the Karoo, but 400 km to the west-southwest of De Aar (Formenti et al., 2002).

Observations in De Aar consisted of solar direct and diffuse radiation measurements by an automated multi-filter rotating shadowband radiometer (MFRSR-7, Yankee Environmental Systems, Turner Falls, Massachusetts). The instrument is described in detail by Harrison et al. (1994) and records irradiation through seven filters. Only five of

Fig. 1. MODIS visual map of South Africa for 14 August 2000, from the Visible Earth site 〈http://visibleearth.nasa.gov/〉, with sunphotometer (yellow) and other locations mentioned in this paper. Image owned by NASA.

these are considered in this study, for wavelengths 415, 501, 615, 673 and 868 nm, and with full width at half maximum (FWHM) ~10 nm.

Measurements commenced on 1 August 2000, and continued until 9 February 2001, with approximately 30 days lost in total (mainly in December and January) due to instrumental problems. Readings of the global and diffuse spectral irradiance were recorded each minute during daylight hours (each reading was actually an average of four measurements made at 15 s intervals).

The solar direct spectral irradiance $F(\lambda)$ is obtained from these by multiplying the difference between the global and diffuse spectral irradiance by the airmass m (airmass is the optical path length through the atmosphere, relative to the zenith path length. It is very close to sec (zenith angle) for not too large zenith angles). The radiation is attenuated according to the Lambert–Beer law $F(\lambda) = F_0(\lambda)\exp(-\tau(\lambda)m)$, where τ is the total optical depth, which is comprised of terms due to Rayleigh scattering (τ_R), absorption by molecules such as ozone and water, and extinction by aerosols (τ_a). Taking logarithms on both sides of the Lambert–Beer equation one attains a straight line relationship referred to as a Langley plot, where the slope of the graph equals τ,

$$\begin{aligned}\ln F &= \ln F_0 - \tau m \\ &= \ln F_0 - (\tau_a + \tau_R + \tau_{ozone} + \tau_{H_2O})m\end{aligned}$$

see e.g. King and Byrne (1976).

In this study we obtained separate Langley plots for each morning and each afternoon (weather conditions permitting), using all data points for airmasses $m = 2$–6. We visually inspected each morning and afternoon sequence to determine the extent to which it was affected by clouds. Where no, or only minor cloud impact was evident, cloud affected readings were removed, and τ values determined through a least-square linear fit to the data for each Langley plot. Sequences with more significant cloud degradation were excluded from further analysis.

The Langley plots generally showed a tight linear correlation of the data points. The linear correlation coefficient R was typically >0.99 for 415 and 501 nm, >0.98 for 615 and 673 nm, and >0.96 for 868 nm. Over the 6 months of study, $\ln F_0$ showed a small, linear upward trend in all filters. Individual discrepancies from the linear trend line very rarely exceeded 1%, again confirming the generally acceptable quality of the data.

We hence obtained 173 aerosol optical depths τ_a per filter by subtracting the Rayleigh and molecular optical depths from τ. We calculated τ_R according to the formula given by Hansen and Travis (1974), and derived the ozone optical depth τ_{ozone} by means of the equation

$$\tau_{ozone}(\lambda) = a_{ozone}(\lambda) \times u_{ozone},$$

where a_{ozone} is the ozone absorption coefficient and u_{ozone} is the atmospheric column ozone concentration. Renzullo (2004) has tabulated these absorption coefficients for the MFRSR-7 filters significantly affected by ozone under a variety of atmospheric conditions (Table 1). In our data reduction we adopt his values for tropical latitudes, which are also almost identical to the corresponding values for summer and winter mid-latitudes.

Table 1
Ozone absorption coefficients for affected MFRSR filters

Band wavelength (nm)	501	615	673
a_{ozone}, λ (mm^{-1})	3.256×10^{-3}	1.189×10^{-2}	4.261×10^{-3}

The ozone concentrations were estimated from the daily Total Ozone Mapping Spectrometer (TOMS) maps 〈http://toms.gsfc.nasa.gov/ozone/ozone.html〉. The water vapour optical depth was neglected, as it does not affect radiation at the wavelengths of the five filters used in the subsequent analysis.

The relation between τ_a and wavelength reveals important information about the particle size distribution of the aerosol. In particular, a plot of $\ln \tau_a$ vs. $\ln \lambda$ is almost linear, and its (negative) slope, α, is referred to as the Angström exponent. This parameter ranges from 0 for the largest to 4 for the tiniest particles, and is thus effectively a measure of the relative importance of the fine mode when compared to the coarse mode. We obtained the Angström exponent using the 415 and 868 nm data, using the relation

$$\alpha = -\frac{\ln \tau_a(415) - \ln \tau_a(868)}{\ln(415) - \ln(868)}.$$

King and Byrne (1976) pointed out that the $\ln \tau_a$ vs. $\ln \lambda$ relationship is better fitted by a quadratic function. The curvature of this function may be parameterised by means of the derivative of the Angström exponent, α', which is also the (negative) second derivative of $\ln \tau_a$ with respect to $\ln \lambda$ (Eck et al., 1999). We here obtained α' by fitting quadratic functions to the $\ln \tau_a$ vs. $\ln \lambda$ curve, and multiplying the coefficient of the $(\ln \lambda)^2$ term by -2. The value of α' increases with larger accumulation mode characteristic radii and with decreasing black carbon concentration (Eck et al., 2001b; O'Neill et al., 2005), and is thus effectively a measure of these parameters.

Complementing the analysis of the aerosol optical depth measurements, back trajectories were calculated using the HYSPLIT4 online programs at 〈www.arl.noaa.gov/ready/hysplit4.html〉 (Draxler and Rolph, 2003; Rolph, 2003) and the FNL database at the National Centres for Environmental Prediction's Global Data Assimilation System. Trajectories extended 5 days backwards, from starting heights of 1450, 1950, 3000, 4200 and 5600 m a.s.l., roughly corresponding to the 850, 800, 700, 600 and 500 hPa pressure levels.

On a small number of occasions, when no obvious source was apparent and mindful of the increased uncertainties thus introduced, trajectories were extended a few days beyond.

3. Results

3.1. Aerosol optical depth time series

Aerosol optical depths were obtained for 173 morning or afternoon sequences. The time series for the entire period of investigation is displayed in Fig. 2. Errors in

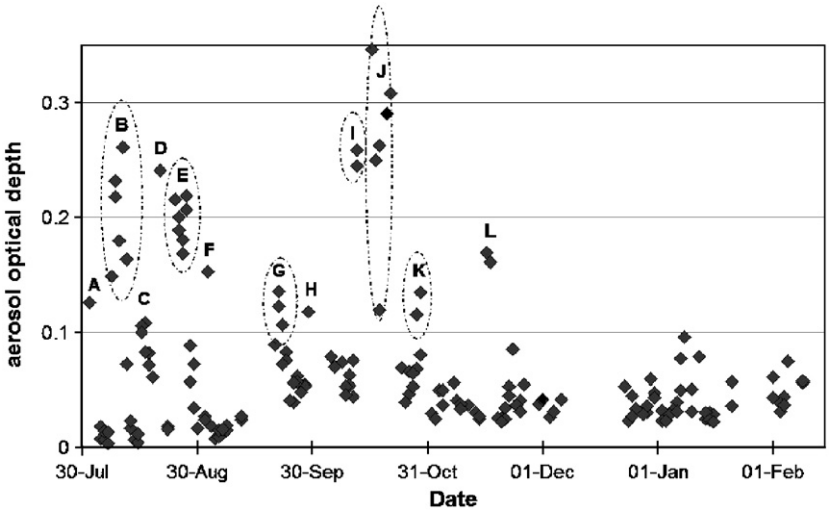

Fig. 2. 415 nm aerosol optical depth for De Aar between 1 August 2000 and 9 February 2001, and identification of 12 events with $\tau_a(415\,\text{nm}) > 0.1$.

individual values of τ_a are expected to be of the order of 0.02 (applying formula (2) of Formenti et al., 2002).

October had the highest monthly average aerosol optical depth, that is $\tau_a(500\,\text{nm}, \text{October}) = 0.10 \pm 0.07$, and an overall Angström exponent of $\alpha = 1.7 \pm 0.3$.

In particular, on a few days De Aar experienced exceptionally low aerosol optical depths of $\tau_a(415\,\text{nm}) < 0.02$ and $\tau_a(868\,\text{nm}) < 0.01$ (4–6 and 13–14 August and 4–6 September 2000). These coincided with wintertime airmasses following the passage of a cold front, and originated over the south Atlantic or even south Pacific oceans, with very little time spent over land.

3.2. Comparison of conditions at different sites

The aerosol optical depths obtained are much lower than those recorded at the various AERONET sites within a 1000 km radius of De Aar, at more polluted locations. Queface et al. (2003) describe data collected at Inhaca island (26°02′S, 32°54′E), where they find an average for October of $\tau_a(500\,\text{nm}, \text{October}) = 0.54$, and an overall Angström exponent of $\alpha = 1.6 \pm 0.2$. They also present data from Bethlehem (28°14′S, 28°19′S,E), obtaining $\tau_a(500\,\text{nm}, \text{October}) = 0.31$, and $\alpha = 1.6 \pm 0.3$.

Elias et al. (2003) presented the results of sunphotometer measurements at Pietersburg (renamed Polokwane) airport (23°53′S, 29°26′E) from 16 August to 18 September 2000. They obtained $\tau_a(868\,\text{nm}) = 0.14 \pm 0.08$, while the Angström exponent fell in the range $\alpha = 1.2$–1.9. For De Aar, the corresponding values for the same period were $\tau_a(868\,\text{nm}) = 0.021 \pm 0.018$ and $\alpha = 1.7$–2.1. We further compare our results with earlier aerosol optical depths recorded at Sutherland (Formenti et al., 2002), where the highest monthly averages were $\tau_a(500\,\text{nm}) = 0.09 \pm 0.08$ (in August 1998) and 0.12 ± 0.10 (in September 1999), while the overall α was determined as 1.8 ± 0.4. Note that the uncertainties quoted in this section denote the scatter in the data, and not the errors of individual measurements.

4. Analysis of maximum and minimum turbidity episodes

We identify 12 events of high aerosol concentrations (i.e. $\tau_a(415\,\text{nm}) > 0.1$), each lasting between 1 and 5 days (see Table 2).

In Fig. 3 we present the plot of α' vs. α for the episodes listed in Table 2. A distinctive clustering of the points associated with particular events is evident in this diagram. In particular, note the close proximity of all events that we later associate with biomass burning to the illustrated straight line.

4.1. Episodes attributed to African biomass burning

Long recognised as the dominant source of haze in the southern African tropics during the fire season (Eck et al., 2001a), biomass smoke was even found responsible for the few instances of significant aerosol loading at Sutherland, in the south-western Karoo (Formenti et al., 2002). Aerosols of this origin can be identified by back trajectories towards tropical Africa or to areas just off the Angolan coast, the expected western limit of the subcontinental circulation system.

For recently formed smoke, α typically takes on values of ~2, or even larger (Dubovik et al., 2002). α' in turn is strongly positive (Eck et al., 1999). Both values decrease for longer-lived particles (e.g. Reid et al., 1998), but the Angström exponent generally stays above 1.2.

Events B, D, E, F, I, J and K (i.e. more than half the high turbidity events) are entirely or predominantly associated with African biomass burning products. Several of the following features are typically observed during these events: (i) high-altitude back trajectories trace a roughly anticyclonic circulation pattern (examples are shown in Fig. 4), (ii) TOMS aerosol index maps show a build-up of particles off the Namibian coast just prior to these events (e.g. 18 August), (iii) high aerosol concentrations are recorded a few days earlier at the Etosha and Mongu

Table 2
Days on which above-average aerosol concentrations were measured

Event	Date (2000)	Time	$\tau_{a,415\,nm}$ (air-mass^{-1})	α	α'	Wind speed (m s^{-1})	Wind direction (°)
A	1 August	a.m.	0.126	1.66	−0.98	n.m.[a]	n.m.[a]
B	7 August	p.m.	0.149	2.04	0.72	0	–
	8 August	a.m.	0.218	1.84	0.47	5	151
	8 August	p.m.	0.232	2.00	0.90	4	316
	9 August	p.m.	0.180	2.03	1.14	2.5	253
	10 August	p.m.	0.261	1.94	0.82	4	261
	11 August	p.m.	0.163	1.80	0.38	5	200
C	15 August	a.m.	0.106	1.71	−1.31	5	160
	16 August	a.m.	0.108	1.74	−0.89	0	–
D	20 August	a.m.	0.241	–	1.20	4	151
E	24 August	p.m.	0.216	2.05	0.71	3	321
	25 August	a.m.	0.189	1.88	0.23	3	170
	25 August	p.m.	0.200	2.07	0.53	4.5	271
	26 August	a.m.	0.168	–	0.76	4	171
	26 August	p.m.	0.181	2.04	0.41	3.5	–
	27 August	a.m.	0.219	1.87	0.45	2	99
	27 August	p.m.	0.207	1.98	0.80	5	275
F	2 September	a.m.	0.153	1.83	−0.16	0	–
G	21 September	a.m.	0.136	1.04	0.08	5	81
	21 September	p.m.	0.123	1.51	0.25	0	–
	22 September	a.m.	0.107	1.21	0.46	2	30
H	29 September	a.m.	0.118	1.51	−0.08	3	61
I	12 October	a.m.	0.245	1.39	−0.29	9	40
	12 October	p.m.	0.259	1.74	0.24	4	345
J	16 October	a.m.	0.347	1.68	0.45	2	309
	17 October	p.m.	0.250	1.70	0.37	6	265
	18 October	a.m.	0.263	1.61	0.27	3	280
	18 October	p.m.	0.119	1.63	0.23	8	285
	20 October	a.m.	0.291	1.59	0.15	4	113
	21 October	a.m.	0.308	1.62	0.08	3	42
K	28 October	p.m.	0.115	1.65	−0.35	2.5	16
	29 October	a.m.	0.135	1.48	0.12	7	330
L	16 November	p.m.	0.169	1.10	−1.23	3.5	46
	17 November	a.m.	0.161	1.40	−0.74	8	20

The meteorological data are from 〈http://meteo.infospace.ru/wcarch/html/index.sht〉. Morning values were recorded at 8:00 h local time, while the afternoon values are averages of the 14:00 and 20:00 h readings.

[a] n.m.: Not measured on that day.

AERONET stations (Eck et al., 2003), (iv) peaks in the aerosol optical depth are observed at the Bethlehem AERONET station (ENE of De Aar) about a day later (e.g. 19–21 August), (v) the positions of these events in the α' vs. α diagram are characteristic of evolved smoke.

Event F occurred at the time of the south-easterly 'River of Smoke' phenomenon mentioned earlier. We note that there is a moderate peak in aerosol concentration over Bethlehem on 2–3 September (Eck et al., 2003), consistent with this pattern. It is thus most likely that the aerosols observed over De Aar during event F are biomass burning products at the edge of the 'River of Smoke'.

We note that AERONET stations in Zambia recorded high aerosol optical depths (AOD) throughout early October (Holben and Eck, 2004; e.g. τ_a(501 nm) at Mongu ranged from ~0.4 to ~1), indicating that southern African biomass burning was still intensive late in the season. The products of these fires were visible over De Aar from 16 to 21 October (event J).

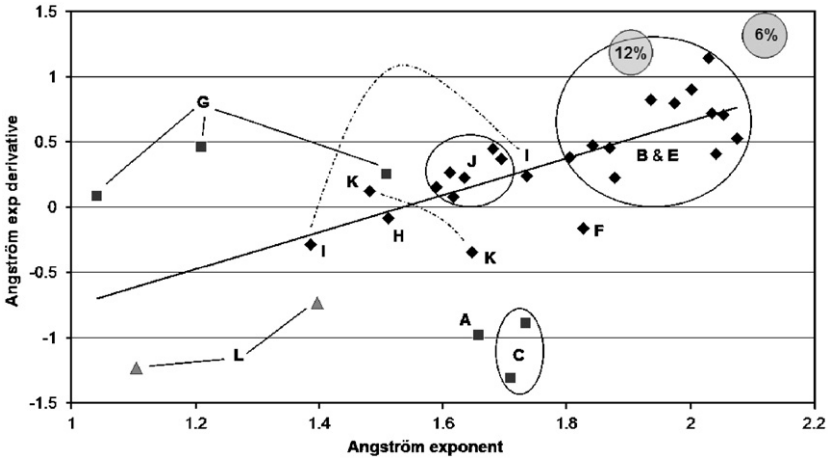

Fig. 3. α' vs. α diagram. Diamonds: biomass burning; squares: Highveld emissions or dust; triangles: unclear. A–L mark the high-aerosol-concentration episodes identified in Table 2 (event D is not plotted as its α' is undefined). The line is the best fit for the biomass burning points. '6%' and '12%' mark the loci of the 6% and 12% soot core mass fractions for 0.1 μm particles, according to O'Neill et al. (2005).

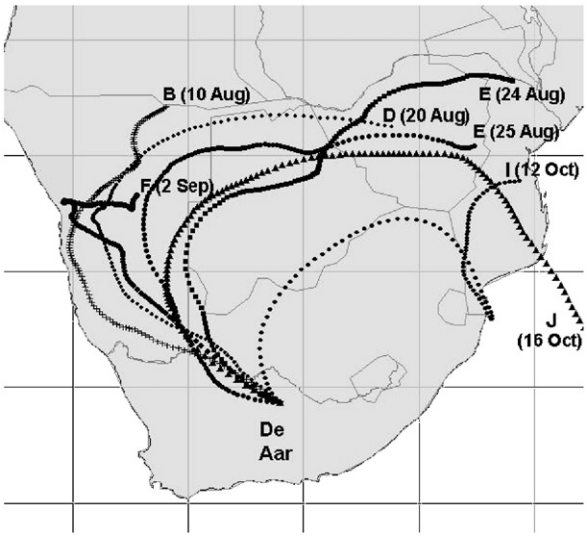

Fig. 4. Selected back trajectories during events associated with African biomass burning. Letters indicate the associated high aerosol concentration events defined in Table 2. Dates refer to detections above De Aar at the following heights: B—500 kPa; D, E, F—700 kPa; I—800 kPa; J—600 kPa; K—850 kPa. Individual points are spaced 1 h apart. The maps in Figs. 4–6 were produced using ArcView GIS software.

Back trajectories for events I and K in October follow a more north-easterly course, and pass Botswana, Zimbabwe and southern Mozambique, where biomass burning takes place later in the spring—see Silva et al. (2003).

Smaller contributions by anthropogenic emissions are possible during the African biomass burning events, as low-level back trajectories often cross parts of the Highveld.

4.2. Episodes attributed to South American biomass burning

There was evidence of occasional transport of smoke from South America in the results of Formenti et al. (2002). The identification of aerosols in this category is conditional on back trajectories extending to areas in the Amazon basin experiencing large-scale fires. Comparisons of African and South American biomass smoke also imply that particles are slightly larger for the latter, and manifest themselves through smaller α-values (Eck et al., 2001a). This may however no longer be applicable when comparing very aged smoke, for which coagulation is no longer significant.

The back trajectory analysis suggests that events H and I were at least in part due to biomass burning products from the Amazon (see Fig. 5). The 500 hPa trajectory for event H crossed the east coast of South America 5 days earlier, south of the Amazon basin, but close enough for this to be considered as the source, given uncertainties in the trajectory calculations. The TOMS maps for 23–25 September indeed show extensive fires in central Brazil. Only moderate aerosol concentrations were recorded at Bethlehem on 29 September, but these increased significantly the following day (Eck et al., 2003), consistent with an eastward-flowing aerosol cloud.

Even though event I has been mainly attributed to southern African biomass burning, we propose that it is partly due to South American fires as well. Some 600 and 500 hPa trajectories corresponding to this event (and for the week before, when aerosol optical depths were <0.1, but above the De Aar mean) extend to Brazil. Three AERONET sites in that area, Abracos Hill, Alta Floresta and Rio Branco, recorded peak aerosol optical depths in the last week of September, so significant generation of aerosols from the Amazon region would be expected. The cross-Atlantic movement of these aerosols is not readily visible on TOMS and MODIS maps for late September due to the very moderate AOT.

4.3. Episodes attributed to anthropogenic emissions

In southern Africa, anthropogenic aerosols are to a great degree associated with emissions on the Highveld, a region of high population density and industrial activity, centred on Johannesburg, and including major mining and

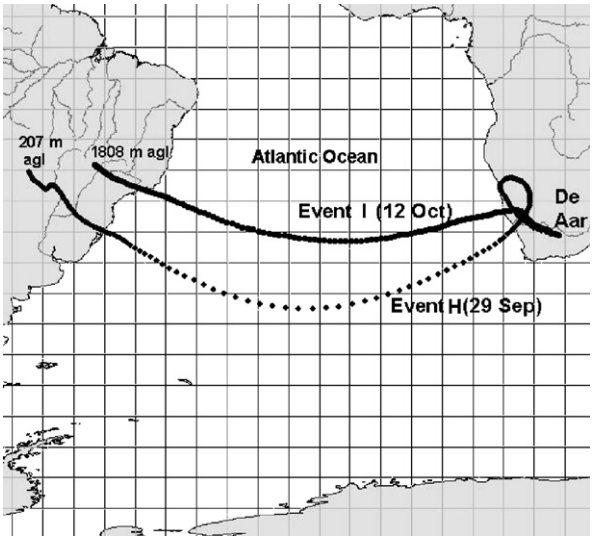

Fig. 5. Selected 8-day back trajectories during events associated with South American biomass burning: 29 September—500 kPa, 12 October—600 kPa. The heights of both starting points are indicated.

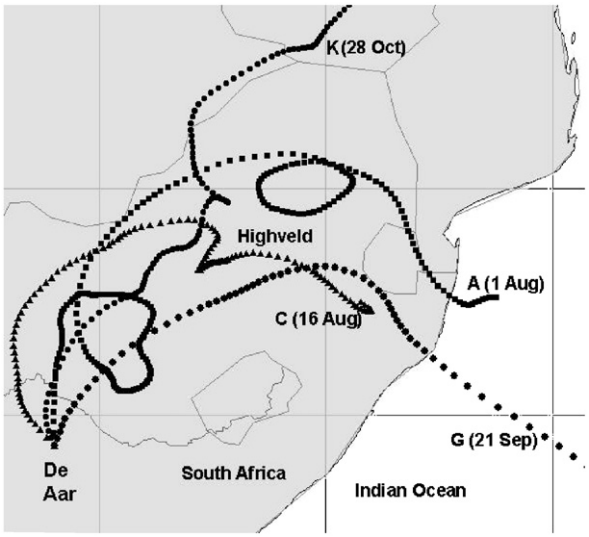

Fig. 6. Selected 850 kPa back trajectories during events associated with anthropogenic emissions, possible marine sources and dust.

power generating areas such as the coal fields around Witbank. The (α, α') signatures for anthropogenic particles generated in this environment are uncertain. Dubovik et al. (2002) quote Angström exponents ranging from 1 to 2.5 for various world cities, averaging at $\alpha = 1.8$. Eck et al. (1999) give α' values widely ranging between -0.22 and 1.76 for Goddard Space Flight Centre in the greater Washington conurbation. In the Karoo, such particles are only expected to be detected in significant numbers when back trajectories cross the Highveld at low altitudes.

We find events C and G to be largely due to anthropogenic emissions, as the low-altitude 850 hPa back trajectories during these periods cross the Highveld at very low altitudes above the ground, and surface winds tend to be from a north-easterly direction (see Fig. 6). These events may also be partly influenced by South American biomass burning, as some high-altitude back trajectories extend in the direction of Brazil. TOMS aerosol maps show significant particle concentrations in the Amazon basin on 7 August as well as 10 September, and a trace of aerosols over the southern mid-Atlantic on 13 August. As the loci of these events in the α' vs. α diagram (Fig. 3) are untypical of aged biomass products, the anthropogenic fractions are however believed to be the dominant.

4.4. Episodes attributed to aeolian dust or other sources

The preparation of agricultural fields for planting in neighbouring Free State province usually takes place around August, at the end of the dry season. The loose soil, denuded of vegetation, is easily raised into dust clouds. A strong wind is, however, required to propel dust and keep it airborne. Dust particles tend to be large, and hence normally have small α and negative α' (Eck et al., 1999). Dubovik et al. (2002) found α values ranging between -0.1 and 1.6, averaging 0.6, for three sites affected by wind-born desert sand. Any soil dust detected at De Aar is expected to arrive from the north-east, i.e. from the direction of the Free State agricultural regions.

We consider event A to be associated with dust (although the relatively large α-value suggests contributions from other sources as well). Dust, haze and high wind speeds from a northerly direction were reported by the De Aar weather station over this period, in particular on 2 August, when cloudiness precluded solar irradiance measurements. The locus of the data point on the α vs. α' diagram is consistent with a bimodal size distribution with a significant coarse mode fraction.

During event L, fresh winds are from the north-east and back trajectories cross the south Indian Ocean and Highveld just above the surface. The α and α' values during this event suggest these aerosols have a comparatively prominent coarse mode. This could be consistent with aeolian dust, though the possibility of marine aerosol (e.g. Andreae et al., 1999) cannot be entirely excluded, despite the relative distance of our site from the coast.

4.5. Days of minimum aerosol concentrations

Table 3 lists the days on which exceptionally low optical depths of $\tau_a(415\,\text{nm}) < 0.02$ and $\tau_a(868\,\text{nm}) < 0.01$ were recorded.

What is common to these periods is that (i) they are all in winter/early spring, (ii) they follow the passage of a cold front, and are therefore associated with colder-than-average conditions, and (iii) all air back trajectories lead to the south Atlantic, with very little time spent over land.

5. Discussion and conclusions

5.1. The southern African sub-continental gyre

Aerosol optical depths at De Aar, at the geographic centre of South Africa, are similar to those recorded at

Table 3
Meteorological conditions on the clearest days

Dates	T (a.m.) (°C)	T (p.m.) (°C)	Wind (m s^{-1})	Wind dir
4–6 August	3.8	13.2	3	NW
13–14 August	6.5	18.3	3	SE
4–6 September	6.9	13.8	2	NW

Sutherland. There is however a clear distinction between results obtained at our sampling site and Bethlehem, 250 km south of Johannesburg (as well as Inhaca and Pietersburg), as aerosol concentrations increase substantially north-east of De Aar. This indicates that the southern boundary of the wintertime sub-continental aerosol-rich airflow is in most instances just north of our location of study.

The results are consistent with trajectories commonly observed in pre-frontal conditions, when air parcels above the boundary layer tend to move in a south-easterly direction between central Namibia and the Highveld. Such local air transport patterns are expected for a regional gyre recirculation model, but may also signify a 'River of Smoke' scenario. Swap et al. (2003) argue that the latter is related to ENSO cycle atmospheric conditions typical of wet years in southern Africa. If this is the case, then a sub-continental recirculation gyre would occur more frequently during drier epochs.

5.2. Amazon biomass burning aerosols crossing the Atlantic

Plumes of aerosols presumed to have been emitted in the Amazon basin and crossing the south Atlantic were reported during the TRACE-A experiment (see, for example, Browell et al., 1996). Formenti et al. (2002) identified South American aerosols with $\tau_a = 0.22$ above Sutherland on 13 September 1999. The likely detections of South American smoke in this work confirm that transport of substantial biomass burning aerosol across the South Atlantic is not uncommon.

It is expected that trans-Atlantic aerosols impact on other southern African sites as well, but their relative concentration will be much lower in areas of large-scale emissions. They are therefore only likely to stand out in the clearer atmospheres well south of the tropics.

5.3. The α' vs. α diagram—a diagnostic tool for characterising aerosols

Analysis of the Angström exponent derivative α' usually focuses on plotting its time series, or comparison with the aerosol optical depth (e.g. Eck et al., 1999). As stated earlier, α' describes accumulation mode particle sizes and black carbon concentrations, while the Angström exponent is an indicator of the relative fine mode strength. An α' vs. α plot is therefore expected to be a suitable diagnostic diagram for identifying different aerosol types.

O'Neill et al. (2005) have calculated the effects of size, aging and humidification on the Angström exponent and its derivative for biomass burning aerosols, and successfully fitted the evolution of smoke from forest fires in Québec with their model. We have marked on the α vs. α' plot (Fig. 3) the locations of 0.1 μm effective radius aerosols with soot cores comprising (i) 6% and (ii) 12% of the total particle mass, as calculated by O'Neill et al.. In their model, aging particles will become displaced towards the loci of larger particles, which they find to be at higher α' and lower α, while increased soot proportions lead to smaller α and α'.

Biomass burning aerosols detected in this study are all aged (>5 days old). They tend to occupy a particular region in Fig. 3, an apparent 'zone of stability' well fitted by the relationship $\alpha' = 1.42\alpha - 2.18$. This part of the diagram cannot immediately be reconciled with the findings of O'Neill et al., particularly for $\alpha' \sim 0$. However, their models only consider fine mode particles, and proved suitable to describe aerosols which developed from unusually intense boreal forest fires in Québec, but are presumably less successful in situations where a considerable coarse mode is present as well.

We hence suggest that the line in Fig. 3 constitutes a good empirical description of aged southern African (and possibly South American) biomass smoke. Comparing our plot with the corresponding diagram in O'Neill et al., we propose that the relative locus of a point along this line is an indicator of the soot fraction in the aerosol.

The high turbidity events attributed to dust, anthropogenic emissions or marine aerosols (A, C, G, L), occupy locations in the diagram associated with stronger coarse mode fractions, and/or different particle compositions. More data are required to define the characteristic photometric features of these other aerosol types.

When comparing sites it should be noted that there may be systematic differences between the parameters α and α' as calculated with our MFRSR, and those obtained using other instruments and filters.

5.4. Meteorological characteristics during 'aerosol-depleted' conditions

In this study we observed several instances of periods during which aerosol concentrations were exceptionally low. All were associated with the presence overhead of cold air originating in the southern oceans. The air is transported to the southernmost parts of Africa in the aftermath of cold fronts, which are typical weather features here during the austral winter.

It is here also worth noting that the days just before the arrival of a cold front tend to coincide with the highest recorded aerosol concentrations. This is because the flow of air from north-west, which is characteristic of strong sub-continental circulation, is enhanced under such circumstances.

5.5. Aerosol type apportionment

Of the 34 sequences with high aerosol optical depth, 76% were found to be caused by biomass burning (73% from African fires and 3% from South American burns).

Eighteen percent are associated with Highveld anthropogenic emissions or dust, while no obvious identification existed for the remaining 6% of cases. Note also that biomass burning aerosols were responsible for the highest aerosol optical depths.

Total aerosol apportionment for the period under investigation, measured in terms of the efficiency in attenuating radiation at 415 nm, was estimated by adding the τ_a(415 nm) values in Table 2 for each aerosol type, divided by the sum of all the recorded values of aerosol optical depth. According to this criterion, for the analysed period biomass burning products contribute 84% to 415 nm irradiation losses due to aerosols over De Aar, dust and anthropogenic emissions 11%, and particles of uncertain origin 5%. Although the data for the relatively clearer days are not included in the derivation of this estimate, they would not affect significantly the overall apportionment.

The above should however not be confused with the mass and volume fractions of the different types of aerosols. A sample of generally small biomass burning aerosols is much more efficient in attenuating light than, say, the same mass of typically larger dust particles. The biomass burning aerosol mass fraction is therefore much smaller than 84%. This is particularly true at lower altitudes, where industrial, aeolian and marine particles are much more pronounced.

Nevertheless, our results, collected over a 6-month period spanning the biomass burning season and much of the following summer, confirm that the aerosols generated through biomass burning are by far the most important aerosol contributor to the radiation balance over the location studied. It is expected that this result can be generalised to the entire Karoo. Due to their increased abundance, biomass burning aerosols therefore make an even more critical impact on this balance as one moves northward into the heart of the sub-continent.

Acknowledgements

The authors thank Brent Holben and the AERONET group at NASA Goddard Space Flight Centre, Greenbelt, Maryland, for making available to us some of their results, and Tom Eck for beneficial discussions. The TOMS maps referred to are produced by NASA/Goddard. We gratefully acknowledge the NOAA Air Resources Laboratory (ARL) for the provision of the HYSPLIT transport and dispersion model and/or READY website 〈http://www.arl.noaa.gov/ready.html〉 used in this publication. Melanie Kneen assisted with the preparation of the figures. H.W. thanks the Environmental Science Department at the University of Virginia, Charlottesville, for hosting him while the paper was written, as well as support from the Southern Africa–Virginia Network Association (SAVANA). Partial funding came from the German Max Planck Society.

References

Andreae, M.O., Elbert, W., Cai, Y., Andreae, T.W., Gras, J., 1999. Journal of Geophysical Research 104 (D17), 21695–21706.

Browell, E.V., Fenn, M.A., Butler, C.F., Grant, W.B., Clayton, M.B., Fishman, J., Bachmeier, A.S., Anderson, B.E., Gregory, G.L., Fuelberg, H.E., Bradshaw, J.D., Sandholm, S.T., Blake, D.R., Heikes, B.G., Sachse, G.W., Singh, H.B., Talbot, R.W., 1996. Ozone and aerosol distributions and air mass characteristics over the South Atlantic basin during the burning season. Journal of Geophysical Research 101 (D19), 24043–24069.

Draxler, R.R., Rolph, G.D., 2003. HYSPLIT (Hybrid Single-Particle Lagrangian Integrated Trajectory) Model Access via NOAA ARL READY Website: 〈http://www.arl.noaa.gov/ready/hysplit4.html〉. NOAA Air Resources Laboratory, Silver Spring, MD.

Dubovik, O., Holben, B., Eck, T.F., Smirnov, A., Kaufman, Y.J., King, M.D., Tanré, D., Slutsker, I., 2002. Variability of absorption and optical properties of key aerosol types observed in worldwide locations. Journal of the Atmospheric Sciences 59, 590–608.

Eck, T.F., Holben, B.N., Reid, J.S., Dubovik, O., Smirnov, A., O'Neill, N.T., Slutsker, I., Kinne, S., 1999. Wavelength dependence of the optical depth of biomass burning, urban, and desert dust aerosols. Journal of Geophysical Research 104 (D24), 31333–31349.

Eck, T.F., Holben, B.N., Ward, D.E., Dubovik, O., Reid, J.S., Smirnov, A., Mukelabai, M.M., Hsu, N.C., O'Neill, N.T., Slutsker, I., 2001a. Characterization of the optical properties of biomass burning aerosols in Zambia during the 1997 ZIBBEE field campaign. Journal of Geophysical Research 106 (D4), 3425–3448.

Eck, T.F., Holben, B.N., Dubovik, O., Smirnov, A., Slutsker, I., Lobert, J.M., Ramanathan, V., 2001b. Column-integrated aerosol optical properties over the Maldives during the northeast monsoon for 1998–2000. Journal of Geophysical Research 106 (D22), 28555–28566.

Eck, T.F., Holben, B.N., Ward, D.E., Mukelabai, M.M., Dubovik, O., Smirnov, A., Schafer, J.S., Hsu, N.C., Piketh, S.J., Queface, A., Le Roux, J., Swap, R.J., Slutsker, I., 2003. Variability of biomass burning aerosol optical characteristics in southern Africa during the SAFARI 2000 dry season campaign and a comparison of single scattering albedo estimates from radiometric measurements. Journal of Geophysical Research 108 (D13), SAF13.

Elias, T., Piketh, S.J., Burger, R., Silva, A.M., 2003. Exploring the potential of combining column-integrated atmospheric polarization with airborne in situ size distribution measurements for the retrieval of an aerosol model: a case study of a biomass burning plume during SAFARI 2000. Journal of Geophysical Research 108 (D13), SAF44.

Esterhuyse, D.J., 2004. Establishment of the South African baseline surface radiation network station at De Aar. M.Sc. Thesis, University of Pretoria, South Africa.

Formenti, P., Winkler, H., Fourie, P., Piketh, S., Makgopa, B., Helas, G., Andreae, M.O., 2002. Aerosol optical depth over a remote semi-arid region of South Africa from spectral measurements of the daytime solar extinction and nighttime stellar extinction. Atmospheric Research 62, 11–32.

Garstang, M., Tyson, P.D., Swap, R.J., Edwards, M., Kållberg, P., Lindesay, J.A., 1996. Horizontal and vertical transport of air over southern Africa. Journal of Geophysical Research 101 (D19), 23721–23736.

Hansen, J., Travis, L., 1974. Light scattering in planetary atmospheres. Space Science Reviews 16, 527–610.

Harrison, L., Michalsky, J., Berndt, J., 1994. Automated multi-filter rotating shadowband radiometer: an instrument for optical depth and radiation measurements. Applied Optics 33, 5118–5125.

Helas, G., Andreae, M.O., Schebeske, G., Le Canut, P., 1995. SA'ARI-94: a preliminary view on results. South African Journal of Science 91, 360–362.

Holben, B.N., Eck, T.F., 2004. SAFARI 2000 AERONET Ground-based Aerosol Data, Dry Season 2000. Data set. Available on-line: 〈http://www.daac.ornl.gov〉 from Oak Ridge National Laboratory Distributed Active Archive Center, Oak Ridge, TN, USA

Holben, B.N., Eck, T.F., Slutsker, I., Tanré, D., Buis, J.P., Setzer, A., Vermote, E., Reagan, J.A., Kaufman, Y.J., Nakajima, T., Lavenu, F., Jankowiak, I., Smirnov, A., 1998. AERONET—a federated instrument network and data archive for aerosol characterisation. Remote Sensing Environment 66, 1–16.

Holben, B.N., Tanré, D., Smirnov, A., Eck, T.F., Slutsker, I., Abuhassan, N., Newcomb, W.W., Schafer, J.S., Chatenet, B., Lavenu, F., Kaufman, Y.J., Van de Castle, J., Setzer, A., Markham, B., Clark, D., Frouin, R., Halthore, R., Karneli, A., O'Neill, N.T., Pietras, C., Pinker, R.T., Voss, K., Zibordi, G., 2001. An emerging ground-based aerosol climatology: aerosol optical depth from AERONET. Journal of Geophysical Research 106 (D11), 12067–12097.

King, M.D., Byrne, D.M., 1976. A method for inferring total ozone content from spectral variation of total optical depth obtained with a solar radiometer. Journal of the Atmospheric Sciences 33, 2242–2251.

Lindesay, J.A., Andreae, M.O., Goldammer, J.G., Harris, G., Annegarn, H.J., Garstang, M., Scholes, R.J., Van Wilgen, B.W., 1996. International Geosphere–Biosphere Programme/International Global Atmospheric Chemistry SAFARI-92 field experiment: background and overview. Journal of Geophysical Research 101 (D19), 23521–23531.

Ohmura, A., Dutton, E.G., Forgan, B., Fröhlich, C., Gilgen, H., Hegner, H., Heimo, A., König-Langlo, G., McArthur, B., Müller, G., Philipona, R., Pinker, R., Whitlock, C.H., Dehne, K., Wild, M., 1998. Baseline Surface Radiation Network (BSRN/WCRP): new precision radiometry for climate research. Bulletin of the American Meteorological Society 79, 2115–2136.

O'Neill, N.T., Thulasiraman, S., Eck, T.F., Reid, J.S., 2005. Robust optical features of fine mode size distributions: application to the Québec smoke event of 2002. Journal of Geophysical Research 110, D11207.

Otter, L.B., Scholes, R.J., Dowty, P., Privette, J., Caylor, K., Ringrose, S., Mukelabai, M., Frost, P., Hanan, N., Totolo, O., Veenendaal, E.M., 2002. The Southern African Regional Science Initiative (SAFARI 2000): wet season campaigns. South African Journal of Science 98, 131–137.

Piketh, S.J., Swap, R.J., Anderson, C.A., Freiman, M.T., Zunckel, M., Held, G., 1999. The Ben Macdhui high altitude trace gas and aerosol transport experiment. South African Journal of Science 95, 35–49.

Queface, A., Piketh, S.J., Annegarn, H., Holben, B., Uthui, R., 2003. Retrieval of aerosol optical thickness and size distribution from Cimel sun photometer over Inhaca Island, Mozambique. Journal of Geophysical Research 108 (D13), SAF45.

Reid, J.S., Hobbs, P.V., Ferek, R.J., Blake, D.R., Martins, J.V., Dunlap, M.R., Liousse, C., 1998. Physical, chemical, and optical properties of regional hazes dominated by smoke in Brazil. Journal of Geophysical Research 103 (D24), 32059–32080.

Renzullo, L.J., 2004. Radiometric processing of multitemporal sequences of satellite imagery for surface reflectance retrievals in change detection studies. Ph.D. Thesis, Curtin University of Technology, Australia.

Rolph, G.D., 2003. Real-time Environmental Applications and Display System (READY) Website: 〈http://www.arl.noaa.gov/ready/hysplit4.html〉. NOAA Air Resources Laboratory, Silver Spring, MD.

Shugart, H.H., Macko, S.A., Lesolle, P., Szuba, T.A., Mukelabai, M.M., Dowty, P., Swap, R.J., 2004. The SAFARI 2000—Kalahari Transect Wet Season Campaign of year 2000. Global Change Biology 10, 273–280.

Silva, J.M.N., Pereira, J.M.C., Cabral, A.I., Sá, A.C.L., Vasconcelos, M.J.P., Mota, B., Grégoire, J.-M., 2003. An estimate of the area burned in southern Africa during the 2000 dry season using SPOT-VEGETATION satellite data. Journal of Geophysical Research 108 (D13), SAF34.

Swap, R.J., Annegarn, H.J., Suttles, J.T., Haywood, J., Helmlinger, M.C., Hely, C., Hobbs, P.V., Holben, B.N., Ji, J., King, M.D., Landmann, T., Maenhaut, W., Otter, L., Pak, B., Piketh, S.J., Platnick, S., Privette, J., Roy, D., Thompson, A.M., Ward, D., Yokelson, R., 2002. The Southern African Regional Science Initiative (SAFARI 2000): overview of the dry season field campaign. South African Journal of Science 98, 125–130.

Swap, R.J., Annegarn, H.J., Suttles, J.T., King, M.D., Platnick, S., Privette, J.L., Scholes, R.J., 2003. Africa burning: a thematic analysis of the Southern African Regional Science Initiative (SAFARI 2000). Journal of Geophysical Research 108 (D13), SAF1.

Tyson, P.D., 1997. Atmospheric transport of aerosols and trace gases over southern Africa. Progress in Physical Geography 21, 79–101.